IEICE TRANS. ELECTRON., VOL.E105–C, NO.11 NOVEMBER 2022

INVITED PAPER *Special Section on Recent Advances in Simulation Techniques and Their Applications for Electronics*

Optimal Design of Optical Waveguide Devices Utilizing Beam Propagation Method with ADI Scheme

Akito IGUCHI[†a)], ***Member and*** **Yasuhide TSUJI**[†], ***Senior Member***

SUMMARY This paper shows structural optimal design of optical waveguide components utilizing an efficient 3D frequency-domain and 2D time-domain beam propagation method (BPM) with an alternating direction implicit (ADI) scheme. Usual optimal design procedure is based on iteration of numerical simulation, and total computational cost of the optimal design mainly depends on the efficiency of numerical analysis method. Since the system matrices are tridiagonal in the ADI-based BPM, efficient analysis and optimal design are available. Shape and topology optimal design shown in this paper is based on optimization of density distribution and sensitivity analysis to the density parameters. Computational methods of the sensitivity are shown in the case of using the 3D semi-vectorial and 2D time-domain BPM based on ADI scheme. The validity of this design approach is shown by design of optical waveguide components: mode converters, and a polarization beam splitter.

key words: *beam propagation method, time-domain beam propagation method, alternating direction implicit method, optical waveguide, shape and topology optimal design*

1. Introduction

Shape and topology optimization is one of the powerful solutions to enhance the performance of optical waveguide components used in optical communication systems. In many reports including authors' group, the validity of this optimization have been shown numerically and experimentally by design of many fundamental components in optical circuits [1]–[16].

Shape and topology optimization is usually based on iteration of numerical simulation and sensitivity analysis to design parameters. As a numerical simulation method, the finite element method (FEM) and the finite difference time/frequency domain (FD-TD/FD) method are widely employed in the design of optical components. The beam propagation method (BPM) [17]–[21] is also broadly used especially for analysis of optical waveguide components in planner lightwave circuit [10]–[13], [22]. Although the BPM is fundamentally an approximation technique based on slowly varying envelope approximation (SVEA), it offers faster and more efficient propagation analysis than rigorous methods like the FEM and the FD-TD/FD. In the 3D-BPM based on FD scheme (3DFD-BPM), the system matrices can be tridiagonal by an alternating direction implicit (ADI) scheme [19]–[21]. Since a tridiagonal system can be solved very efficiently by the so called Thomas algorithm, the 3D-BPM with the ADI scheme can contribute to efficient 3D design. We developed gradient-based shape and topology optimal design approach utilizing semi- and full-vectorial 3DFD-BPM with the ADI scheme in [14], [15]. This design approach using semi-vectorial FD-BPM can easily be applied to the case of using the 2D time-domain FD-BPM (TDFD-BPM) [16]. The TDFD-BPM which applies the SVEA to time-axis overcomes the drawback of the usual BPM, it also can be efficient by using the ADI scheme in 2D analysis [23]. The optimal design using the 2DTD-BPM with the ADI scheme can contribute to initial design of optical components in high-index-contrast waveguides. Moreover, the design approach using the TD-BPM is useful to get wavelength-flattened response because in the TD-BPM multi-wavelength response can be taken into account by one propagation analysis of a modulated pulse.

In this paper, we show a design strategy utilizing BPM methods with the ADI scheme for optical waveguide components. This paper takes into account the semi-vectorial 3D design problem in frequency domain analysis, and 2D design problem in time-domain analysis. In our approach, shape and topology optimization is carried out by solving optimization problem of density parameters which is allocated at each discrete cell. The density parameters are updated iteratively using a gradient method based on sensitivity of figure of merit (FoM). This paper describes sensitivity analysis method in the case of using the semi-vectorial 3DFD-BPM and the 2DTD-BPM with ADI scheme, and the validity of the computed sensitivity is verified by design of optical components.

In Sect. 2, we describe the design strategy based on sensitivity analysis, and briefly review sensitivity analysis method in the case of using the BPMs with the ADI scheme. In Sect. 3, we apply our design approach to 3D or 2D design of optical components, and show the numerical validation of this design approach. As design examples, we design mode converters in low-index-contrast waveguide and a polarization beam splitter (PBS) in high-index-contrast platform using the 3D-BPM and the 2DTD-BPM, respectively. This paper is concluded in Sect. 4.

2. Design Strategy Using ADI-Based BPM

2.1 Optimal Design Procedure

In this section, the design procedure based on sensitivity

Manuscript received October 31, 2021.
Manuscript revised January 14, 2022.
Manuscript publicized May 20, 2022.

[†]The authors are with Muroran Institute of Technology, Muroran-shi, 050–8585 Japan.
a) E-mail: iguchia@mmm.muroran-it.ac.jp

DOI: 10.1587/transele.2021ESI0001

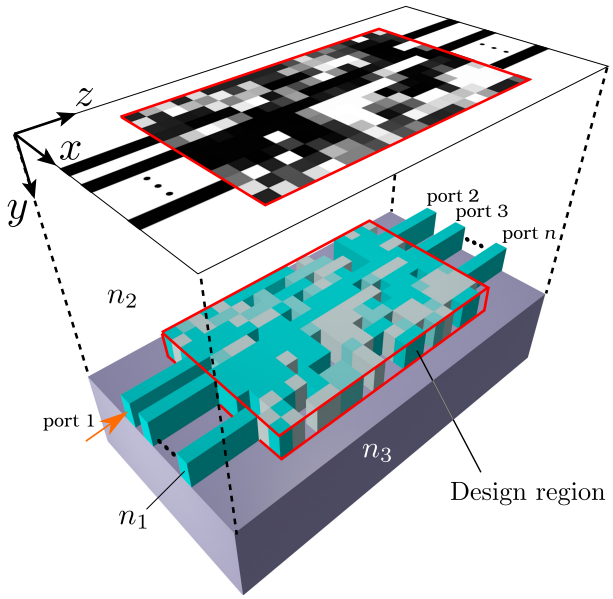

Fig. 1 Design model of optical waveguide devices.

analysis utilizing the BPM is described. A 3D design and analysis model considered in this paper is shown in Fig. 1. n_1, n_2, and n_3 are refractive indices of core, cover cladding, and substrate materials, respectively. The computational window is discretized by step size Δx, Δy, Δz in $x-$, $y-$, $z-$direction. We represent the material distribution using normalized density parameter ρ as follows:

$$n^2(i,j,k) = n_2^2 + (n_1^2 - n_2^2)U(\rho(i,j,k), P) \tag{1}$$

where $n(i,j,k) \equiv n(i\Delta x, j\Delta y, k\Delta z)$ is refractive index, and $\rho(i,j,k) \equiv \rho(i\Delta x, j\Delta y, k\Delta z)$ is normalized density allocated at each discrete cell. The FD cell whose central point is $(i\Delta x, j\Delta y, k\Delta z)$ is filled by the material whose refractive index is $n(i\Delta x, j\Delta y, k\Delta z)$. $U(\rho, P) \in [0,1]$ is a quasi-step function depending on penalty parameter P:

$$U(\rho, P) = \begin{cases} 0.5(2\rho)^P & [0 \le \rho \le 0.5] \\ 1 - 0.5(2-2\rho)^P & [0.5 < \rho \le 1] \end{cases}. \tag{2}$$

In this paper, we solve minimization problem of objective function instead of maximization problem of FoM. To compute sensitivity of objective function, the derivative $\partial n^2/\partial\rho$ has to be calculated. To let n^2 differentiable, $U(\rho, P)$ has transition region from 0 to 1. Figure 2 shows relation between the quasi-step function and P. Δ_ρ indicates gray area where $U(\rho, P) \in [0.01 : 0.99]$. The gray area can be shrunk by making P large. P is small value in the initial phase of optimization, and it is increased gradually. In the final phase, P is made be large enough to remove gray area, and it is almost wiped out when $P = 400$ where Δ_ρ is less than 0.01. In 3D design problems, we assume the height of waveguide core is uniform in design region. In 2D design, we optimize material distribution in $x - z$ cross section including waveguide core.

We summarize the flow of the design approach as follows:

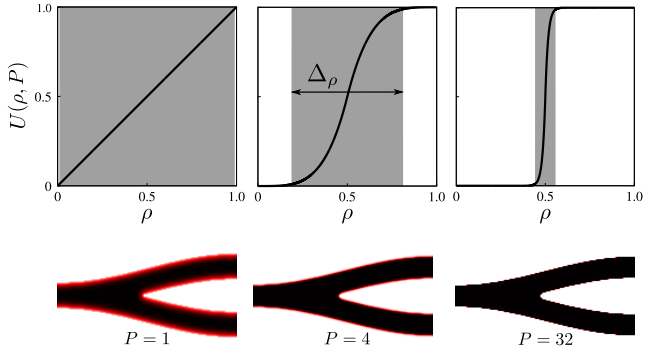

Fig. 2 A quasi-step function $U(\rho, P)$ depending on penalty parameter P. Red painted-region indicates gray material which has intermediate refractive index between core and cladding materials.

1. Determine initial distribution of ρ and P.
2. For iteration count $i = 0, 1, 2, \cdots$, do:
   a. FoM of an optical component is evaluated using the BPM with ADI scheme, and compute objective function f_i.
   b. Compute sensitivity of objective function to ρ.
   c. Update ρ using a gradient method based on computed sensitivity.
   d. If $i \neq 0$ and $|f_i - f_{i-1}| < \epsilon$, the penalty parameter increases: $P \leftarrow \alpha P$ $(1 < \alpha)$.
   e. If $P_{\max} < P$, stop the iteration.

In the rest part of this section, we describe sensitivity analysis method in the case of using the BPM with ADI scheme. In addition, we offer detail description about the update of density distribution.

2.2 Sensitivity Analysis Using the BPM Based on ADI Scheme

First, we describe sensitivity analysis method using the semi-vectorial 3D-BPM. In the semi-vectorial problem, the govern equation is the following wave equation extracted from Maxwell equation:

$$\frac{\partial^2\Phi(x,y,z)}{\partial z^2} + (D_{xx} + D_{yy} + \nu)\Phi(x,y,z) = 0 \tag{3}$$

where Φ is electro-magnetic (EM) field, $\nu = k_0^2 n^2$, and k_0 is wavenumber in free space. D_{xx}, D_{yy} are operators depending on Φ:

$$D_{\alpha\alpha}\Phi = \begin{cases} \frac{\partial^2 H_\alpha}{\partial\alpha^2} & [\Phi = H_\alpha] \\ n^2 \frac{\partial}{\partial\alpha}\left(\frac{1}{n^2}\frac{\partial H_\beta}{\partial\alpha}\right) & [\Phi = H_\beta] \end{cases} \tag{4}$$

where $(\alpha, \beta) \in [(x,y),(y,x)]$.

In the frequency-domain BPM, a time-harmonic EM field Φ is factorized by [17]:

$$\Phi(x,y,z) = \phi(x,y,z)\exp(-\mathrm{j}\beta_0 z) \tag{5}$$

where z is considered as propagation direction of lightwave, β_0 is a reference phase constant, and $\mathrm{j} = \sqrt{-1}$. ϕ is slowly

varying EM field in $z-$direction when the difference between actual phase constant β and β_0 is small enough. Applying (5) to (3) and employing Crank-Nicolson FD scheme and ADI scheme, the update equation in the implicit BPM can be derived [20]:

$$[\Gamma_2]_k \{\phi\}_{k+1/2} = [\Gamma_1]_k \{\phi\}_k \tag{6}$$

$$[\Gamma_4]_k \{\phi\}_{k+1} = [\Gamma_3]_k \{\phi\}_{k+1/2} \tag{7}$$

where $[\Gamma_m]_k\,(m = 1,2,3,4)$ is a propagator matrix in $z-$direction, and $\{\phi\}_k$ is a vector representation of $\phi(x,y)$ at $z = k\Delta z$. The propagating wave is computed sequentially by the two-step linear systems. From (6) and (7), the relation between EM fields at input plane and endface, $\{\phi\}_0$ and $\{\phi\}_{N_z}$, can be expressed by:

$$\{\phi\}_{N_z} = \Pi_{k=0}^{N_z-1} [P]_k \{\phi\}_0 \tag{8}$$

$$[P]_k = [\Gamma_4]_k^{-1} [\Gamma_3]_k [\Gamma_2]_k^{-1} [\Gamma_1]_k\,. \tag{9}$$

Note that we here define that Π is reverse order product:

$$\Pi_{k=0}^{N} [P]_k = [P]_N \cdots [P]_1 [P]_0\,. \tag{10}$$

When FoM of optical components depends on S-parameters, its sensitivity has to be computed to calculate $\partial f/\partial\rho$. An S-parameter can be represented by:

$$S_{n1} = \iint_\Omega \psi_n^*(x,y)\phi(x,y,N_z\Delta z)dxdy = \{\psi_n\}^\dagger \{\phi\}_{N_z} \tag{11}$$

where n is an output port number, ψ_n is an evaluated eigenmode field at port n. $\{\psi_n\}$ is a vector related to ψ_n, and superscript † indicates conjugate transpose. From (8), the sensitivity of S_{n1} to density parameters can be represented by:

$$\begin{aligned}\frac{\partial S_{n1}}{\partial\rho(i,j,k)} &= \{\psi_n\}^\dagger \frac{\partial \{\phi\}_{N_z}}{\partial\rho(i,j,k)} \\ &= \{\psi_n\}^\dagger [P]_{N_z-1} \cdots [P]_{k+1} \\ &\quad \cdot \frac{\partial [P]_k}{\partial\rho(i,j,k)} [P]_{k-1} \cdots [P]_0 \{\phi\}_0\,.\end{aligned} \tag{12}$$

Eventually, we get the following relation:

$$\begin{aligned}\frac{\partial S_{n1}}{\partial\rho(i,j,k)} &= -\{\lambda\}_{k+1}^T \frac{\partial [\Gamma]_4}{\partial\rho(i,j,k)} \{\phi\}_{k+1} \\ &\quad + \{\lambda\}_{k+1}^T \frac{\partial [\Gamma]_3}{\partial\rho(i,j,k)} \{\phi\}_{k+1/2} \\ &\quad - \{\lambda\}_{k+1/2}^T \frac{\partial [\Gamma]_2}{\partial\rho(i,j,k)} \{\phi\}_{k+1/2} \\ &\quad + \{\lambda\}_{k+1/2}^T \frac{\partial [\Gamma]_1}{\partial\rho(i,j,k)} \{\phi\}_k\end{aligned} \tag{13}$$

where superscript ^{T} indicates transpose. $\{\lambda\}_{k+1}$ and $\{\lambda\}_{k+1/2}$ can be represented by the following linear systems:

$$[\Gamma_4]_k^T \{\lambda\}_{k+1} = [P]_{k+1}^T \cdots [P]_{N_z-1}^T \{\psi_n\}^* \tag{14}$$

$$[\Gamma_2]_k^T \{\lambda\}_{k+1/2} = [\Gamma_3]^T \{\lambda\}_{k+1} \tag{15}$$

where superscript * indicates complex conjugate.

This procedure of sensitivity analysis can be applied to the case of using 2DTD-BPM with ADI scheme in the same fashion. In the 2DTD-BPM, the slowly varying axis is let to be time-axis [24]:

$$\Phi(x,z,t) = \phi(x,z,t)\exp(\mathrm{j}\omega_0 t) \tag{16}$$

where $\Phi \in (E_y, H_y)$, and ω_0 is a reference angular frequency. Although we omit the details, applying narrow-band approximation, the following relation can be obtained as with the case of 3D-BPM [23]:

$$\{\phi\}_{N_t} = [P]^{N_t} \{\phi\}_0 \tag{17}$$

$$[P] = [\Gamma_4]^{-1} [\Gamma_3] [\Gamma_2]^{-1} [\Gamma_1] \tag{18}$$

where $\{\phi\}_{N_t}$ is a vector representation of $\phi(x,z,N_t\Delta t)$, and Δt is time step. In (17), it is assumed that material distribution is time-invariant. $\{\phi\}_0$ is an initial state of input pulse in port 1, and Gaussian pulse is usually employed. N_t is taken to be time step where peak of the following value is observed.

$$c_n = \left| \int_\Gamma \psi_n^* \phi(x,z,\tau\Delta t) d\Gamma \right|^2 \tag{19}$$

where Γ is observed plane of output pulse. Instead of an S-parameter, the following coefficient is employed to evaluate FoM of optical components.

$$\eta_{n1} = \iint_\Omega \psi_n^*(x,z)\phi(x,z,N_z\Delta z)dxdz = \{\psi_n\}^\dagger \{\phi\}_{N_t} \tag{20}$$

where $\psi_n^*(x,z)$ is an ideal state at $t = N_t\Delta t$ of output pulse in port n, and $\{\psi_n\}$ is its vector representation. Sensitivity of η_{n1} to density parameter can be computed by:

$$\begin{aligned}\frac{\partial \eta_{n1}}{\partial\rho(i,k)} = \sum_{\tau=0}^{N_t} \Bigg[&-\{\lambda\}_{\tau+1}^T \frac{\partial [\Gamma]_4}{\partial\rho(i,k)} \{\phi\}_{\tau+1} \\ &+ \{\lambda\}_{\tau+1}^T \frac{\partial [\Gamma]_3}{\partial\rho(i,k)} \{\phi\}_{\tau+1/2} \\ &- \{\lambda\}_{\tau+1/2}^T \frac{\partial [\Gamma]_2}{\partial\rho(i,k)} \{\phi\}_{\tau+1/2} \\ &+ \{\lambda\}_{\tau+1/2}^T \frac{\partial [\Gamma]_1}{\partial\rho(i,k)} \{\phi\}_\tau \Bigg]\end{aligned} \tag{21}$$

with

$$[\Gamma_4]^T \{\lambda\}_{\tau+1} = ([P]^T)^{N_t-1-\tau} \{\psi_n\}^* \tag{22}$$

$$[\Gamma_2]^T \{\lambda\}_{\tau+1/2} = [\Gamma_3]^T \{\lambda\}_{k+1}\,. \tag{23}$$

2.3 Update of Density Parameters

In 3D design, the sensitivity is summed up in $y-$axis so as to make the core height uniform in the design region:

$$\frac{\partial f}{\partial \rho(i,k)} = \sum_{j=M_b}^{M_t} \frac{\partial f}{\partial \rho(i,j,k)} \tag{24}$$

where $y = M_t \Delta y$ and $M_b \Delta y$ are top and bottom position of the design region. In addition, in order to avoid extremely complicated material distribution, a simple moving average is applied to the sensitivity map as follows:

$$F\left(\frac{\partial f}{\partial \rho(i,k)}\right) = \sum_{\alpha=-1}^{1} \sum_{\beta=-1}^{1} \frac{1}{9} \frac{\partial f}{\partial \rho(i+\alpha, k+\beta)}. \tag{25}$$

To minimize f, we update ρ based on the sensitivity using a steepest descent method as follows:

$$\rho(i,k) \leftarrow \rho(i,k) - K \cdot F\left(\frac{\partial f}{\partial \rho(i,k)}\right) \tag{26}$$

where K is update step size, and we determine that in this paper $K = \delta / \max_{i,k} \partial f / \partial \rho(i,k)$ where δ is maximum variation of the density per one iteration. We tune the parameters α, δ, ϵ so that an objective function is surely converged.

3. Design Examples

In this section, first, using the 3DFD-BPM, we design mode converters which can be passive components of the mode multiplexer/demultiplexer in mode-division-multiplexing (MDM) system. Next, using the 2DTD-BPM, we design the PBS which is employed to control polarization state of lightwave and an essential component in high-index-contrast optical circuits.

3.1 Mode Converters

First, we design a $TE_0(E_{11}^x)$-to-$TE_1(E_{21}^x)$ mode order converter using the semi-vectorial 3D-BPM. Figure 3 is the design schematic of the mode order converter. The refractive indices are $n_1 = 1.466$, $n_2 = n_3 = 1.444$, and core width and height are taken to be $w = 8\ \mu$m and $h = 6\ \mu$m, respectively. The size of the design region is taken to be $D_x = 50\ \mu$m, $D_z = 805\ \mu$m. D_z is determined by a sizing optimized mode order converter based on cascaded period grating [27], [28], which is made to be an initial profile. The objective function to be minimized is determined so that an incident TE_0 wave at wavelength of 1.55 μm is converted into TE_1 wave:

$$\text{minimize } f = \left(1 - \left|S_{21(\text{TE0}\to\text{TE1})}\right|^2\right)^2 \tag{27}$$

where $\left|S_{21(\text{TE0}\to\text{TE1})}\right|^2$ is normalized power of TE_1 wave at port 2 when TE_0 wave is launched into port 1. Although backward reflection cannot taken into account in the standard BPM, it is negligibly small because the profile of the device designed here is slowly varying in z-direction, and the design model is low-index-contrast system. The transversal computational domain is enclosed by the perfectly matched layer (PML) [25], [26], and its thickness is set to be 5 μm. The step sizes in $x-$, $y-$, and $z-$ direction are $\Delta x = \Delta y = 0.1\ \mu$m and $\Delta z = 1\ \mu$m, respectively. Δx and Δy are determined so that effective indices of TE_0 and TE_1 modes are not so varied even if smaller step size is chosen. Since an unknown field ϕ is slowly-varying field in z-direction, larger Δz is allowed if it can be predicted that an actual phase constant is in the vicinity of the reference phase constant.

The normalized objective function (f/f_0) as a function of iteration count is shown in Fig. 4. The black vertical dashed lines indicate changing points of the penalty parameter P, and it is changed from 4 to 400. One can see that the objective function decreases with iteration except for changing points of P, thus valid sensitivity is evaluated. Figure 5 shows the initial concept and the optimized profile of mode order converters. The launched TE_0 wave is surely converted into TE_1 wave in both converters. The power transmission spectra is shown in Fig. 6. In the optimized converter, power transmission of TE_1 wave is > -0.149 dB at C-band, whereas > -0.896 dB in the initial converter. The crosstalk which is defined by ratio of power transmission of TE_0 to that of TE_1 is < -21.3 dB in the initial converter, and < -21.4 dB in the optimized one at C-band. The optimized converter achieves lower insertion loss than the initial one maintaining low crosstalk.

Next, we design a $LP_{11a}(E_{21}^x)$-to-$LP_{11b}(E_{12}^x)$ mode rotator which requires 3D analysis and design. Figure 7 is the design schematic of the higher-order mode rotator. The up-

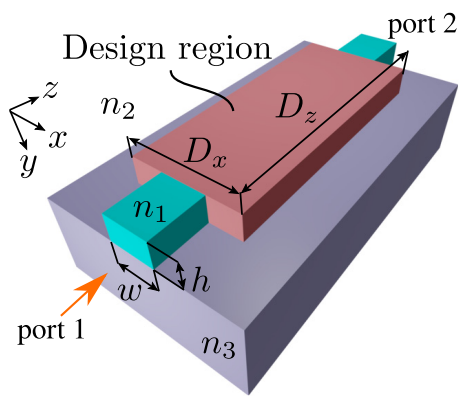

Fig. 3 3D design schematic of TE_0-to-TE_1 mode order converter.

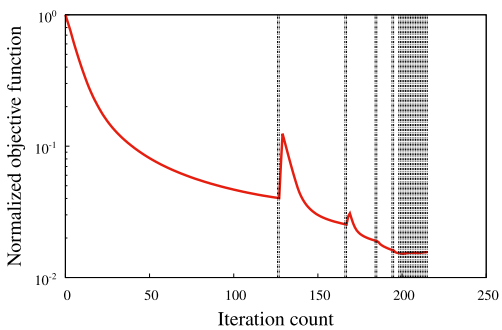

Fig. 4 Normalized objective function in design of TE_0-to-TE_1 mode order converter. The black vertical dashed lines indicate changing points of penalty parameter P.

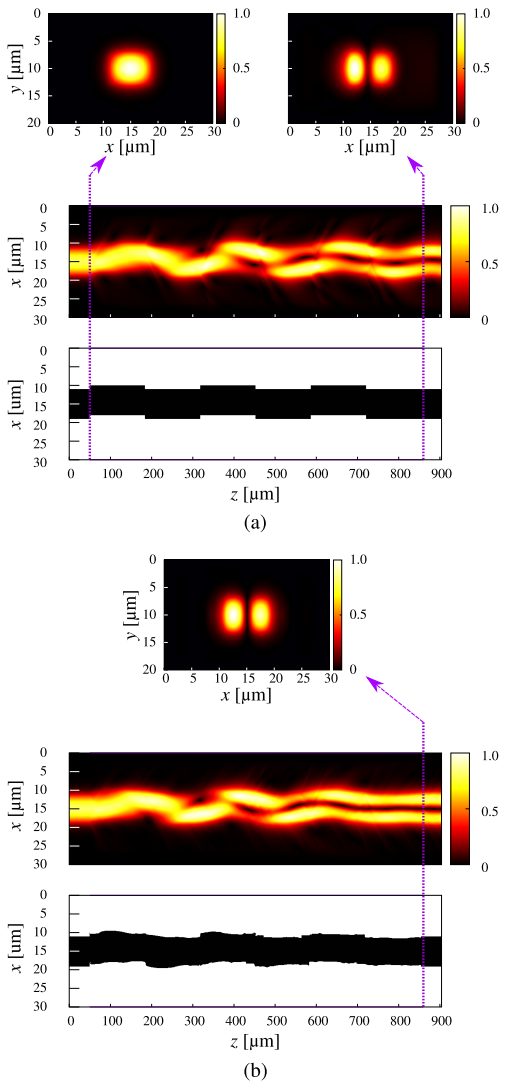

Fig. 5 Designed TE_0-to-TE_1 mode order converters and propagating wave ($|H_y|$). (a) The initial concept. (b) The optimized profile. The propagating wave is computed at wavelength of 1.55 μm.

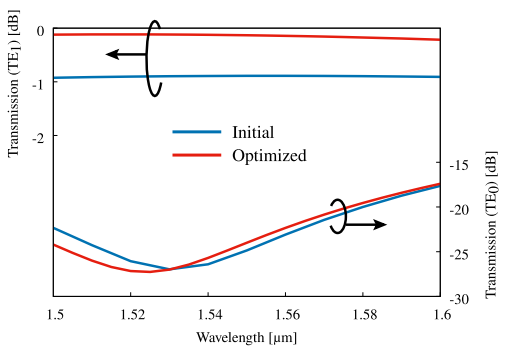

Fig. 6 Power transmission spectra of mode order converters.

per half layer is taken to be the design region so as to break horizontal symmetry and induce mode rotation. The refractive indices are the same as the previous design example, and core width and height are taken to be $w = h = 6$ μm.

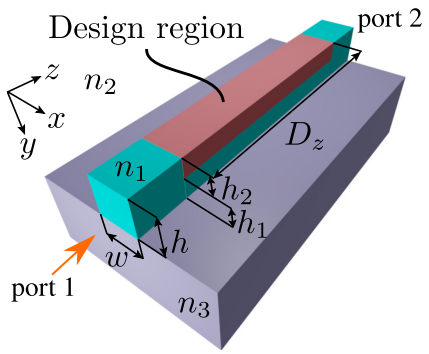

Fig. 7 3D design schematic of LP_{11a}-to-LP_{11b} mode rotator.

The thickness of upper and bottom layers are made to be the same: $h_1 = h_2 = h/2$. The objective function is determined so that an incident LP_{11a} wave at wavelength of 1.55 μm is converted into LP_{11b} wave:

$$\text{minimize } f = \left(1 - \left|S_{21(\text{LP11a}\rightarrow\text{LP11b})}\right|^2\right)^2 \tag{28}$$

where $\left|S_{21(\text{LP11a}\rightarrow\text{LP11b})}\right|^2$ is normalized power of LP_{11b} wave at port 2 when LP_{11a} wave is launched into port 1. The initial profile of the rotator is based on a trench-assisted mode rotator reported in [29], [30], and longitudinal size of the design region D_z is taken to be 371 μm which is determined by beating length of two super modes excited in the trench-assisted core. The PML thickness and step sizes in the BPM analysis are the same as the previous example.

Figure 8 is the design results of the mode rotator. It can be seen that the trench profile is adjusted so that mode rotation efficiency is improved, and almost completely LP_{11b} mode profile can be seen in the optimized mode rotator. Figure 9 is power transmission spectra of the initial and the optimized mode rotators. The initial mode rotator has LP_{11b} power transmission of > -0.777 dB at C-band, and the optimized one has the higher transmission of > -0.142 dB. The crosstalk which is defined by ratio of power transmission of LP_{11a} to that of LP_{11b} is < -22.7 dB in the initial rotator, and < -22.0 dB in the optimized one at C-band. Also in this design example, higher mode conversion efficiency is accomplished maintaining low crosstalk.

3.2 Polarization Beam Splitter

Third example is a 2D design of a polarization beam splitter (PBS) in high-index-contrast platform using TD-BPM. The design schematic is shown in Fig. 10, and the structural parameters are taken to be as follows: $n_1 = 2.2$, $n_2 = 1.444$, $w = 0.5$ μm, $D_x = 5$ μm, $D_z = 20$ μm, and $s = 2.5$ μm. In this design example, an initial concept is not given, and a simple sinusoidal Y-branching waveguide is made to be an initial profile. The following Gaussian pulse is employed as an input pulse at $t = 0$ s:

$$\phi(x,z) = \phi_1(x)\exp\left\{\frac{(z-z_0)^2}{4}\right\}\exp\left(-\mathrm{j}k_0 n_e z\right) \tag{29}$$

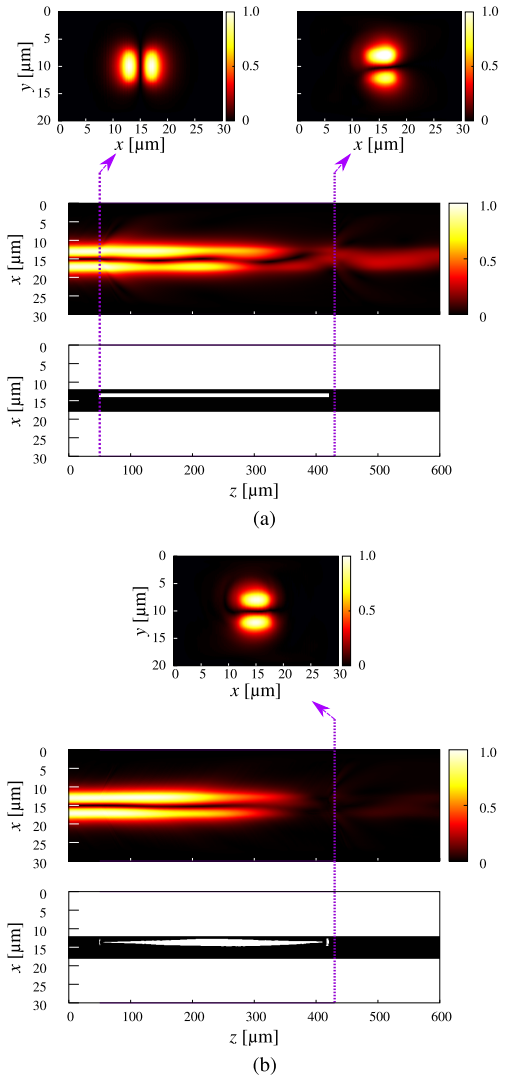

Fig. 8 Designed LP_{11a}-to-LP_{11b} mode rotators and propagating wave ($|H_y|$). (a) The initial concept and (b) the optimized profile in the upper layer ($7 < y < 10\ \mu$m). The propagating wave is computed at wavelength of 1.55 μm. Cross section at $y = 10\ \mu$m is shown in $x - z$ plane of $|H_y|$.

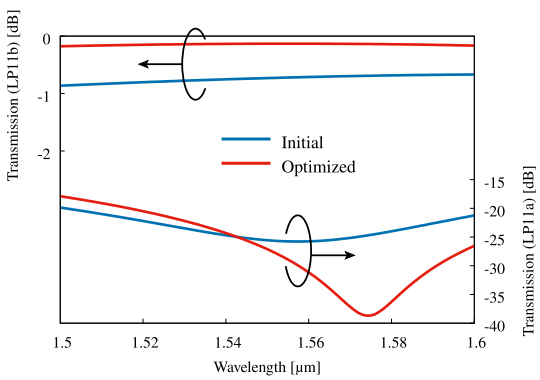

Fig. 9 Power transmission spectra of mode rotators.

where $\phi_1(x)$ is an eigenmode field in port 1, n_e is its effective index, and z_0 is central position of the pulse which is taken to be $z_0 = 6\ \mu$m. $\Gamma_{i/o}$ is observed plane of the input and

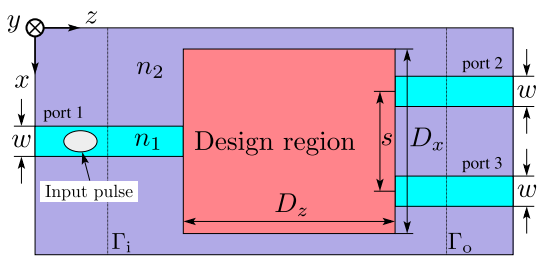

Fig. 10 2D design schematic of a polarization beam splitter.

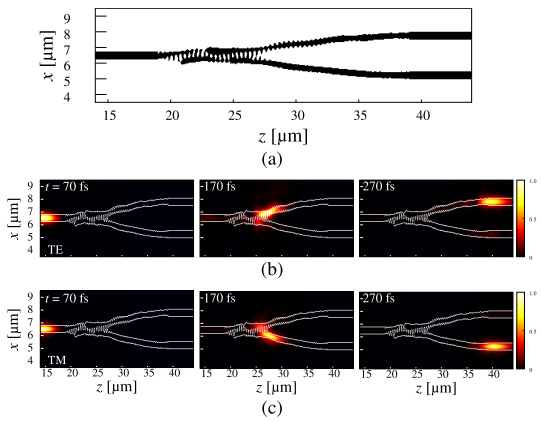

Fig. 11 Designed PBS and propagating wave. (a) The optimized PBS, propagation (b) TE and (c) TM pulse waves at $t = 70,\ 170,\ 270$ fs.

the output pulse. The observed positions are set to be $z = 11.5$ and 44 μm. The computational domain is enclosed by the PML with thickness of 0.5 μm in $x-$direction and 1 μm in $z-$direction. The step sizes in $x-$ and $z-$ direction are $\Delta x = \Delta z = 0.05\ \mu$m, and the time step is set to be $\Delta t = 1$ fs. The objective function is determined so that $TE_0(TM_0)$ pulse wave with central wavelength of 1.55 μm is output to port 2(port 3):

$$\text{minimize } f = f_{\text{PBS}} + f_{\text{XT}} \tag{30}$$

$$f_{\text{PBS}} = (1 - |\eta_{21(\text{TE0})}|^2)^2 + (1 - |\eta_{31(\text{TM0})}|^2)^2$$

$$f_{\text{XT}} = \left(0 - \frac{|\eta_{31(\text{TE0})}|^2}{|\eta_{21(\text{TE0})}|^2}\right)^2 + \left(0 - \frac{|\eta_{21(\text{TM0})}|^2}{|\eta_{31(\text{TM0})}|^2}\right)^2$$

where f_{PBS} is a term to achieve function of the PBS, and f_{XT} is one to reduce crosstalk.

Figure 11 shows the optimized PBS and propagation pulse waves. One can see that the optimized profile has like a grating-assisted directional coupler in the vicinity of the junction. TE and TM waves divided into different ports, and the PBS function is achieved. Figure 12 is power transmission spectra in the optimized PBS. In the shown wavelength range, low insertion loss of > -0.225 dB and low crosstalk of < -20.9 dB are attained. Although 3D design is required so as to estimate out-of-plane radiation, this design approach with the TD-BPM may useful to extract an initial concept with wavelength-flattened spectra in costly 3D design.

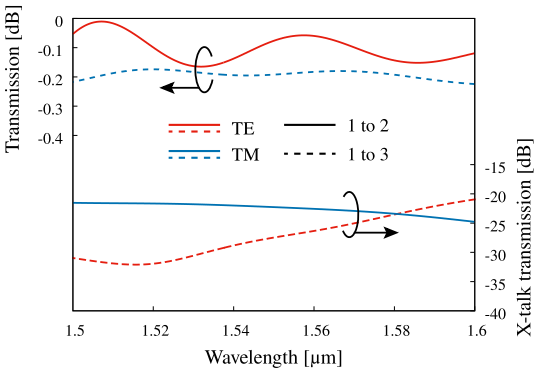

Fig. 12 Power transmission spectra of the designed PBS.

4. Conclusion

In this paper, we showed the design approach utilizing the 3D frequency-domain and 2D time-domain BPMs based on ADI scheme, and a sensitivity analysis technique to density parameters was described in the case of using the ADI-based BPMs. The validity of the computed sensitivity was shown in the design example of mode converters using the semivectorial 3D-BPM. In addition, we showed that the design approach using the BPM based on ADI scheme can be applied to the case of using the 2D TD-BPM. Our design approach successfully achieved improvement of performance of optical waveguide components, and extract device profile which has desired function.

Acknowledgments

This work was supported by JSPS (Japan) KAKENHI Grant Number 20K22408.

References

[1] J.S. Jensen and O. Sigmund, "Systematic design of photonic crystal structures using topology optimization: Low-loss waveguide bends," Appl. Phys. Lett., vol.84, no.12, pp.2022–2024, March 2004.
[2] P.I. Borel, L.H. Frandsen, A. Harpøth, M. Kristensen, J.S. Jensen, and O. Sigmund, "Topology optimised broadband photonic crystal Y-splitter," Electron. Lett., vol.41, no.2, pp.69–71, Jan. 2005.
[3] Y. Tsuji and K. Hirayama, "Design of optical circuit devices using topology optimization method with function-expansion-based refractive index distribution," IEEE Photon. Technol. Lett., vol.20, no.12, pp.982–984, June 2008.
[4] J.L.P. Ruiz, I. Aldaya, P. Dainese, and L.H. Gabrielli, "Design of compact arbitrary-ratio multimode power splitters based on topological derivative," IEEE Photon. Technol. Lett., vol.32, no.18, pp.1187–1190, Sept. 2020.
[5] M. Tomiyasu, K. Morimoto, A. Iguchi, and Y. Tsuji, "A study on function-expansion-based topology optimization without gray area for optimal design of photonic devices," IEICE Trans. Electron., vol.E103-C, no.11, pp.552–559, Nov. 2020.
[6] L.H. Frandsen, Y. Elesin, L.F. Frellsen, M. Mitrovic, Y. Ding, O. Sigmund, and K. Yvind, "Topology optimized mode conversion in a photonic crystal waveguide fabricated in silicon-on-insulator material," Opt. Express, vol.22, no.7, pp.8525–8532, April 2014.
[7] A.Y. Piggott, J. Lu, K.G. Lagoudakis, J. Petykiewicz, T.M. Babinec, and J. Vučković, "Inverse design and demonstration of a compact and broadband on-chip wavelength demultiplexer," Nature Photon., vol.9, pp.374–377, May 2015.
[8] J. Lu and J. Vučković, "Nanophotonic computational design," Opt. Express., vol.21, no.11, pp.13351–13367, June 2013.
[9] M. Perestjuk, H. Boerma, A. Schindler, P. Runge, and M. Schell, "Inverse design strategies for large passive waveguide structures," IEEE Photon. Technol. Lett., vol.33, no.5, pp.259–262, March 2021.
[10] Y. Sakamaki, T. Saida, T. Hashimoto, and H. Takahashi, "New optical waveguide design based on wavefront matching method," J. Lightw. Technol., vol.25, no.11, pp.3511–3518, Nov. 2007.
[11] Y. Sakamaki, T. Saida, T. Shibata, Y. Hida, T. Hashimoto, M. Tamura, and H. Takahashi, "Y-branch waveguides with stabilized splitting ratio designed by wavefront matching method," IEEE Photon. Technol. Lett., vol.18, no.7, pp.817–819, April 2006.
[12] Y. Sakamaki, T. Saida, T. Hashimoto, S. Kamei, and H. Takahashi, "Loss reduction of waveguide crossings by wavefront matching method and their application to integrated optical circuits," J. Lightw. Technol., vol.27, no.13, pp.2257–2263, July 2009.
[13] Y. Sakamaki, S. Kamei, T. Hashimoto, T. Kitoh, and H. Takahashi, "Loss uniformity improvement of arrayed-waveguide grating with mode-field converters designed by wavefront matching method," J. Lightw. Technol., vol.27, no.24, pp.5170–5715, Dec. 2009.
[14] A. Iguchi, Y. Tsuji, T. Yasui, and K. Hirayama, "Efficient topology optimization of optical waveguide devices utilizing semi-vectorial finite-difference beam propagation method," Opt. Express, vol.25, no.3, pp.28210–28222, Nov. 2017.
[15] A. Iguchi, Y. Tsuji, T. Yasui, and K. Hirayama, "Efficient shape and topology optimization based on sensitivity analysis for optical waveguide devices utilizing full-vectorial BPM," J. Lightw. Technol., vol.38, no.8, pp.2328–2335, April 2020.
[16] A. Iguchi, Y. Tsuji, T. Yasui, and K. Hirayama, "Topology optimal design for optical waveguides using time domain beam propagation method," IEICE Electron. Express, vol.15, no.11, 20180417, pp.1–7, May 2018.
[17] M.D. Feit and J.A. Fleck, "Light propagation in graded-index optical fibers," Appl. Opt., vol.17, no.24, pp.3990–3998, Dec. 1978.
[18] Y. Chung and N. Dagli, "An assessment of finite difference beam propagation method," IEEE J. Quantum. Electron., vol.26, no.8, pp.1335–1339, Aug. 1990.
[19] J. Yamauchi, T. Ando, and H. Nakano, "Beam-propagation analysis of optical fibres by alternating direction implicit method," Electron. Lett., vol.27, no.18, pp.1663–1665, Aug. 1991.
[20] P.L. Liu and B.J. Li, "Semivectorial beam-propagation method for analyzing polarized modes of rib waveguides," IEEE J. Quantum. Electron., vol.28, no.4, pp.778–782, April 1992.
[21] Y. Hsueh, M. Yang, and H. Chang, "Three-dimensional noniterative full-vectorial beam propagation method based on the alternating direction implicit method," J. Ligthw. Technol., vol.17, no.11, pp.2389–2397, Nov. 1999.
[22] M. Takahashi, Y. Uchida, S. Yamasaki, J. Hasegawa, and T. Yagi, "Development of low loss ultra-high Δ ZrO_2-SiO_2 PLC for next generation compact and high-density integrated devices," IEICE Trans. Electron., vol.E97-C, no.7, pp.725–730, July 2014.
[23] J. Shibayama, M. Muraki, J. Yamauchi, and H. Nakano, "Comparative study of several time-domain methods for optical waveguide analyses," J. Lightw. Technol., vol.23, no.7, pp.2285–2293, July 2005.
[24] P-L. Liu, Q. Zhao, and F-S. Choa, "Slow-wave finite-difference beam propagation method," IEEE Photon. Technol. Lett., vol.7, no.8, pp.890–892, Aug. 1995.
[25] W.C. Chew and W.H. Weedon, "A 3D perfectly matched medium from modified maxwell's equations with stretched coordinates," Microw. Opt. Technol. Lett., vol.7, no.13, pp.599–604, Sept. 1994.
[26] W.P. Huang, C.L. Xu, W. Lui, and K. Yokoyama, "The perfectly matched layer (PML) boundary condition for the beam propagation method," IEEE Photon. Technol. Lett., vol.8, no.5, pp.649–651, May

1996.
[27] Q. Liu, K.S. Chiang, and V. Rastogi, "Analysis of corrugated long-period gratings in slab waveguides and their polarization dependence," J. Lightw. Technol., vol.21, no.12, pp.3399–3405, Dec. 2003.
[28] Y. Yang, K. Chen, W. Jin, and K.S. Chiang, "Widely wavelength-tunable mode converter based on polymer waveguide grating," IEEE Photon. Technol. Lett., vol.27, no.18, pp.1985–1988, Sept. 2015.
[29] K. Saitoh, T. Uematsu, N. Hanzawa, Y. Ishizaka, K. Masumoto, T. Sakamoto, T. Matsui, K. Tsujikawa, and F. Yamamoto, "PLC-based LP_{11} mode rotator for mode-division multiplexing transmission," Opt. Express, vol.22, no.16, pp.11917–19130, Aug. 2014.
[30] N. Hanzawa, K. Saitoh, T. Sakamoto, T. Matsui, K. Tsujikawa, T. Uematsu, and F. Yamamoto, "PLC-Based four-mode multi/demultiplexer with LP_{11} mode rotator on one chip," J. Lightw. Technol., vol.33, no.6, pp.1161–1165, March 2015.

Akito Iguchi received the B.S., M.S., and Ph.D. degrees in electronic engineering from Muroran Institute of Technology, Muroran, Japan, in 2015, 2017, and 2019. From 2019 to 2020, he was a Post-Doctoral Research Fellow of Japan Society for the Promotion of Science (JSPS). He is currently an Assistant Professor at Muroran Institute of Technology. Dr. Iguchi is a member of the Institute of Electronics, Information and Communication Engineers (IEICE), the IEEE, and the Optical Society of America (OSA).

Yasuhide Tsuji received the B.S., M.S., and Ph.D. degrees in electronic engineering from Hokkaido University, Sapporo, Japan, in 1991, 1993, and 1996, respectively. In 1996, he joined the Department of Applied Electronic Engineering, Hokkaido Institute of Technology, Sapporo, Japan. From 1997 to 2004, he was an Associate Professor of Electronics and Information Engineering at Hokkaido University. From 2004 to 2011, he was an Associate Professor of Electrical and Electronic Engineering at Kitami Institute of Technology, Kitami, Japan. Since 2011, he has been a Professor of Information and Electronic Engineering at Muroran Institute of Technology, Muroran, Japan. He has been interested in wave electronics. Dr. Tsuji is a Senior Member of the Institute of Electronics, Information and Communication Engineers (IEICE), the IEEE, and the Optical Society of America (OSA), and a Member of the Japan Society of Applied Physics. In 2021, He has received the Electronics Society Award form IEICE. In 1997, 1999, and 2019, he was awarded the Best Paper Award from IEICE. In 2000, he has received the Third Millennium Medal from IEEE. In 2019, he has received the IEEE Photonics Technology Letters Outstanding Reviewer Award.